

Needle stylet with integrated optical fibers for spectroscopic contrast during peripheral nerve blocks

Adrien E. Desjardins
Marjolein van der Voort
Stefan Roggeveen
Gerald Lucassen
Walter Bierhoff
Benno H. W. Hendriks
Marcus Brynolf
Björn Holmström

Needle stylet with integrated optical fibers for spectroscopic contrast during peripheral nerve blocks

Adrien E. Desjardins,^a Marjolein van der Voort,^a Stefan Roggeveen,^a Gerald Lucassen,^a Walter Bierhoff,^a Benno H. W. Hendriks,^a Marcus Brynolf,^b and Björn Holmström^{b,c}

^aPhilips Research, Eindhoven, The Netherlands

^bKarolinska University Hospital, Department of Anesthesiology and Intensive Care, B31 Huddinge, SE-141 86 Stockholm, Sweden

^cKarolinska Institutet, Department of Clinical Science, Intervention and Technology, Stockholm, Sweden

Abstract. The effectiveness of peripheral nerve blocks is highly dependent on the accuracy at which the needle tip is navigated to the target injection site. Even when electrical stimulation is utilized in combination with ultrasound guidance, determining the proximity of the needle tip to the target region close to the nerve can be challenging. Optical reflectance spectroscopy could provide additional information about tissues that is complementary to these navigation methods. We demonstrate a novel needle stylet for acquiring spectra from tissue at the tip of a commercial 20-gauge needle. The stylet has integrated optical fibers that deliver broadband light to tissue and receive scattered light. Two spectrometers resolve the light that is received from tissue across the wavelength range of 500–1600 nm. In our pilot study, measurements are acquired from a postmortem dissection of the brachial plexus of a swine. Clear differences are observed between spectra acquired from nerves and those acquired from adjacent tissue structures. We conclude that spectra acquired with the stylet have the potential to increase the accuracy with which peripheral nerve blocks are performed. © 2011 Society of Photo-Optical Instrumentation Engineers (SPIE). DOI: 10.1117/1.3598852

Keywords: spectroscopy; infrared spectroscopy; fiber optic sensors; spectrometers; medicine; optical properties.

Paper 10465RR received Aug. 22, 2010; revised manuscript received Apr. 27, 2011; accepted for publication May 19, 2011; published online Jul. 18, 2011.

1 Introduction

Accurate navigation of the needle tip is critical for ensuring effective outcomes in peripheral nerve blocks. With many peripheral nerve blocks, the target region is the loose adipose tissue surrounding the target nerve; ideally, the injectate spreads around and diffuses into the target nerve. The proximity of the needle tip to the nerve has long been advocated as a positive predictor of patient outcome.¹ Common methods of nerve localization are limited in their effectiveness, however. Mechanical paresthesia was traditionally advocated to verify needle-tip placement, but as a method for detecting nerve contact, it has low sensitivity.² Electrical stimulation can be effective and is recommended for needle-tip localization,³ but it may not elicit a response even when the needle is in physical contact with or is inserted into a nerve.^{4,5} Additionally, electrical stimulation may not be relevant in patients with muscular or neural dysfunction. The limitations of these methods can result in failed blocks. An average failure rate of 20% for peripheral nerve blocks was reported by Grau et al.⁶ and failure rates as high as 30% have been reported specifically for brachial plexus blocks.⁷

Image guidance can significantly improve the outcome of peripheral nerve blocks, offering in certain cases direct visualization of nerves and adjacent anatomical structures. In particular, ultrasound utilized in combination with electrical stimulation can give rise to success rates in the range of 55–100%, depending on the context.⁸ Ultrasound has several limitations that can

limit its range of applicability, however. For instance, ultrasound may not always adequately determine the location of the needle tip as “inside” or “outside” the nerve.⁹ Moreover, visualization of small nerves deep within tissues can be limited by low signal-to-noise and image resolution, particularly with obese patients; bones can give rise to shadows that preclude visualization of nerves beneath them. Both magnetic resonance imaging¹⁰ and computed tomographic scanning¹¹ provide clear visualization of the brachial plexus, but they are time consuming and impractical for guidance in routine procedures. A study of fluoroscopy as a modality for guiding brachial plexus blocks yielded promising results,¹² but further investigations are required to quantify the risk of arterial or lung punctures with that method.

Optical coherence tomography (OCT) is an imaging modality that allows for cross-sectional images to be acquired directly from the needle tip. An optical analog of ultrasound utilizing the principles of low-coherence interferometry, OCT can provide two- and three-dimensional images of tissue with an imaging depth of ~1.5 mm. OCT probes can have simple designs that are compatible with needles as small as 31 gauge.¹³ OCT was applied in preliminary studies to brachial plexus neurovascular structures,^{14,15} to peripheral nerves,¹⁶ and to cavernous nerves of the prostate.^{17,18} Additional studies are required to determine whether OCT is relevant for guiding peripheral nerve blocks. Currently, OCT systems do not provide robust contrast for endogenous chromophore concentrations, so that the information that they provide is to a large extent distinct from spectroscopic measurements. Exogenous chromophores, such as fluorescent

Address all correspondence to: Björn Holmström, Karolinska University Hospital, B31 Huddinge, SE-141 86 Stockholm, Sweden; Tel: 46 858582923; Fax: 46 87795424; E-mail: bjorn.holmstrom@karolinska.se.

retrograde nerve tracers, might be valuable for visualizing nerves when utilized in conjunction with imaging modalities closely related to OCT, such as confocal fluorescence microscopy¹⁹ and reflectance-mode microscopy,²⁰ but the sensitivity, specificity, and practicality of that method in a clinical context remain to be determined.

Optical reflectance spectroscopy with visible and near-infrared (NIR) light could provide information that is not directly available from peripheral nerve stimulators and image guidance. It can identify differences in the concentrations of chromophores, such as hemoglobins, water, and lipids.²¹ With a typical probe configuration, broadband light is delivered to tissue at one location and a portion of the scattered light is received at another location and spectrally resolved. The intensity of the received light depends on the optical absorption of tissue: with higher optical absorption, the intensity of received light is lower, and vice versa. The wavelength-dependencies of the optical absorption spectra differ among prominent tissue chromophores. Oxy- and deoxy-hemoglobin both absorb prominently in the blue and green regions of the visible electromagnetic spectrum (400–750 nm) and in the short-wave NIR range (750–1100 nm); lipids and water absorb prominently in the midwave NIR range (1100–2500 nm).

Recent advances in fiber-optic sensing technologies have enabled miniature optical spectroscopy probes that are integrated into needles. Depending on the optical design, the probes can be “forward-looking,” allowing for measurements predominantly from tissue at the bevel surface,^{22–27} or “side-looking,” targeting tissues close to the aperture of a biopsy needle.^{28,29} As demonstrated in two studies, a needle stylet (the insert that is positioned in the outer hollow cannula to prevent tissue and fluids from entering) can allow for spectroscopic measurements of the epidural space.^{30,31} Some designs allow for measurements of tissue autofluorescence as well.³² The general concept of introducing fiber-optic sensors into a needle stylet was introduced nearly half a century ago, with a coherent fiber bundle for imaging through a 15-gauge hypodermic needle.³³

There is scant scientific literature on the use of optical reflectance spectroscopy for identifying peripheral nerves. Spectroscopy in the NIR spectral range was applied by Bu et al.³⁴ to identify motor and sensory fascicles of dogs, by Xie et al.³⁵ to identify the anterior and posterior roots of *cauda equina* nerves of dogs, by Abdo and Sahin³⁶ to identify peripheral nerves of rats, and by Radhakrishnan et al.^{37,38} to identify sciatic nerves of rats. These preliminary studies suggested that peripheral nerves can potentially be differentiated from surrounding tissues with optical reflectance spectroscopy, but the measurement probes were incompatible with percutaneous procedures.

In this study, we present a custom-designed needle stylet that allowed for the acquisition of spectra from tissues at the tip of a 20-gauge needle. As a preliminary investigation of the spectra associated with nerves and surrounding tissues, spectra were acquired from a postmortem dissection of the brachial plexus of a swine.

2 Methods

The needle stylet was designed to be used in combination with a commercial 20-gauge injection needle with a 900- μm o.d. and a shaft length of 100 mm (Terumo Corporation, Tokyo,

Japan). It was developed from a solid stainless steel rod with a 550 μm o.d. Three optical fibers were integrated along the long axis of the rod so that their distal ends terminated at the bevel surface. They were mounted with epoxy into grooves that were created in the rod with spark erosion (Fig. 1). The distal end faces of the optical fibers were perpendicular with respect to the fiber axes; they were positioned within the grooves so that they contacted the bevel surface of the stylet but did not protrude beyond it. The angles of the bevel surfaces of the stylet and cannula, measured relative to the long axis of the stylet, were 18 and 20 deg, respectively. The former angle was chosen to be slightly smaller than the latter to ensure that the stylet did not protrude beyond the bevel surface of the cannula.

Each optical fiber was 150 μm diam with a 100- μm -diam core. One optical fiber in the stylet delivered broadband light from a tungsten-halogen lamp (HL-2000-HP, Ocean Optics, Dunedin, Florida) to the needle tip. This light was scattered and absorbed by the tissue; a portion was received by the two other fibers. With this probe geometry, the delivery fiber is optically isolated from the collection fibers and, therefore, light that is specularly reflected from the delivery fiber is not received. Each collection fiber was positioned 1 mm from the delivery

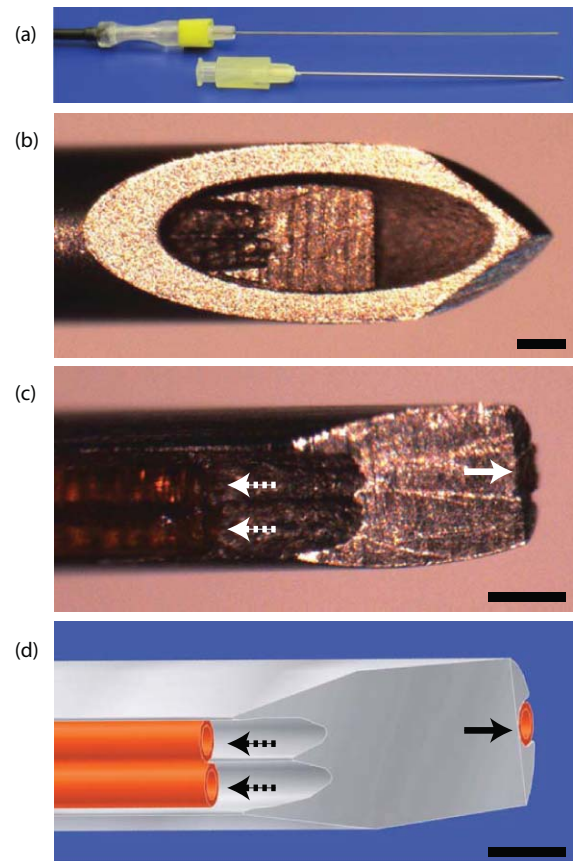


Fig. 1 (a) Stylet with integrated optical fibers (top) and corresponding needle cannula (bottom). (b) Close-up of the distal end of the cannula with the stylet fully inserted. The bevel surface of the stylet is visible within the oval opening of the cannula. (c,d) Close-up of the needle stylet in the absence of the cannula, shown as a photo and a schematic. The distal ends of the fiber for delivering light and the fibers for receiving light are identified with the solid and dashed arrows, respectively. Scale-bar: 250 μm .

fiber, with this distance measured from the centers of the distal end faces of the fibers along the surface of the stylet bevel (Fig. 1). At the proximal end of the stylet, the fibers exited at a plastic port that was designed to be compatible with the female Luer Lock connector on the needle cannula. From their point of exit at the port to the connectors at which they terminated, the optical fibers were enclosed in an optically opaque protective flexible sheath.

Light received from tissue was directed to two spectrometers, where it was spectrally resolved. Each spectrometer comprised a compact spectrograph (Shamrock 163, Andor Technology, Belfast, United Kingdom). Light in the range of 500–1000 nm was detected with a silicon array (DU420A-BR-DD, Andor Technology, Belfast, United Kingdom) in the first spectrometer; light in the range of 900–1600 nm was detected with an InGaAs sensor array (DU492A-1.7, Andor Technology, Belfast, United Kingdom) in the second. Both sensors were cooled to -50°C during operation to minimize dark currents. With both spectrometers, the spectral resolution was ~ 7 nm. The spectrometer system, which included a laptop computer for data acquisition, was previously described.³⁹ Processing of spectra was performed offline with custom software written in MATLAB (The MathWorks, Natick, Massachusetts).

The average maximum penetration distance attained by light as it propagates from the delivery fiber to one of the collection fibers depends on the interfiber distance. To determine the average maximum penetration distance and its wavelength dependency, Arifler et al. recently performed a detailed study with Monte Carlo modeling of light propagation in epithelial and stromal tissue.⁴⁰ It was found that for a probe configuration that was similar to the one in our study, with fiber diameters of $200\ \mu\text{m}$ and an interfiber distance of 1.1 mm, the average maximum penetration distances at wavelengths of 375, 500, and 625 nm were 0.7, 0.9, and 1.1 mm, respectively. By linear extrapolation of these results, a coarse estimate of the average maximum penetration distance at the near-infrared wavelength of 1000 nm was found to be 1.5 mm. For wavelengths at which water absorption is very high, such as those of > 1400 nm, linear extrapolation of the results of Arifler et al. is likely to be inaccurate; the average maximum penetration distance is expected to be $\ll 1.5$ mm.

Spectra were acquired with the needle stylet positioned in the cannula, from tissue structures in and surrounding the brachial plexus of a Swedish Landrace swine (42 kg, male), at the axillary level. The swine had been sacrificed for experiments with objectives distinct from those of this study. The surgical dissection commenced immediately postmortem. During the acquisition of spectra, the stylet was held manually by the practitioner. For each location of the needle tip, a set of 10 spectra was acquired, with the bevel surface of the stylet in direct contact with the tissue surface. The needle-tip locations were classified as follows: (i) inside skeletal muscle; (ii) on the surface of an artery, (iii) on the surface of a vein, (iv) at the nerve target region before the surrounding fascia layer and extraneural fibrofatty connective tissue was removed, (v) at the nerve target region after the surrounding fascia layer and extraneural fibrofatty connective tissue was removed, and (vi) inside the nerve after penetrating ~ 0.5 mm below the surface. In case (vi), the dissection technique did not allow for the position of the bevel surface relative to fascicles within the nerve to be determined. For each class of

needle-tip location, spectra were acquired at four different positions that were evenly distributed across the dissection field. Each spectrum was acquired in 0.5 s.

To investigate the extent to which spectra from different classes of tissue structures differed, a multivariate statistical data reduction algorithm was utilized. The algorithm produced two spectrum classifiers for each optical reflectance spectrum with a combination of principal components analysis (PCA) and linear discriminant analysis (LDA). This combination is commonly utilized to analyze optical spectra acquired from tissue.^{41–43} Prior to the first step of the algorithm, each spectrum was normalized by dividing all intensities by the mean intensity of that spectrum. In the first step, PCA was applied to extract four parameters from each spectrum. With PCA, a spectrum is represented as a sum of principal components (PCs), with each PC weighted by a parameter called a component score. Taken together, the first few component score parameters typically account for a large fraction of the total variance in the spectra. In the second step, LDA was applied to the set of four parameters obtained from PCA to obtain two spectrum classifiers, SC1 and SC2, which are optimal from the standpoint of classification.⁴⁴ As such, the PCA-LDA algorithm provides a two-dimensional representation of spectra that emphasizes differences between spectra that are obtained from different tissue structures.

3 Results

Spectra acquired from each class of needle-tip location are shown in Fig. 2. They are plotted as the mean intensity of light received by the needle in linear units, as a function of the light wavelength. The standard deviations, plotted relative to the mean, are measures of the variability of the intensity of light received when the needle was held manually at the location from which the spectra were acquired. Absorption peaks, which manifested as lower light intensities in specific spectral regions, corresponded well to the absorption peaks of certain known chromophores. In all spectra, absorption peaks in the range of 500–600 nm were consistent with hemoglobin absorption.⁴⁵ Both oxygenated and deoxygenated forms of hemoglobin and/or myoglobin were observed, with the former form associated with a single absorption peak at 557 nm and a less prominent absorption peak centered at 757 nm, and the latter associated with two absorption peaks at 542 and 576 nm. An absorption peak at 1210 nm and a much less prominent one at 930 nm were consistent with the presence of lipids.^{46,47} Absorption peaks centered at 976, 1197, and 1455 nm were consistent with water absorption;⁴⁸ of the three, the latter was particularly prominent.

Lipid absorption peaks at 1210 nm were prominent in all spectra acquired from the nerve target regions and from within the nerves; they appeared particularly prominent in spectra acquired from the surfaces of nerves and from the interiors of nerves. These lipid absorption peaks were visually absent in spectra acquired from skeletal muscle and from the surfaces of arteries and veins. With spectra acquired from the surfaces of veins, water absorption peaks were particularly prominent, as were hemoglobin absorption peaks in the range of 500–600 nm and the deoxy-hemoglobin peak at 757 nm.

Spectra acquired from different positions on the surfaces of nerves are shown in Fig. 3. These plots provide qualitative indications of the extent to which the shapes of spectra varied

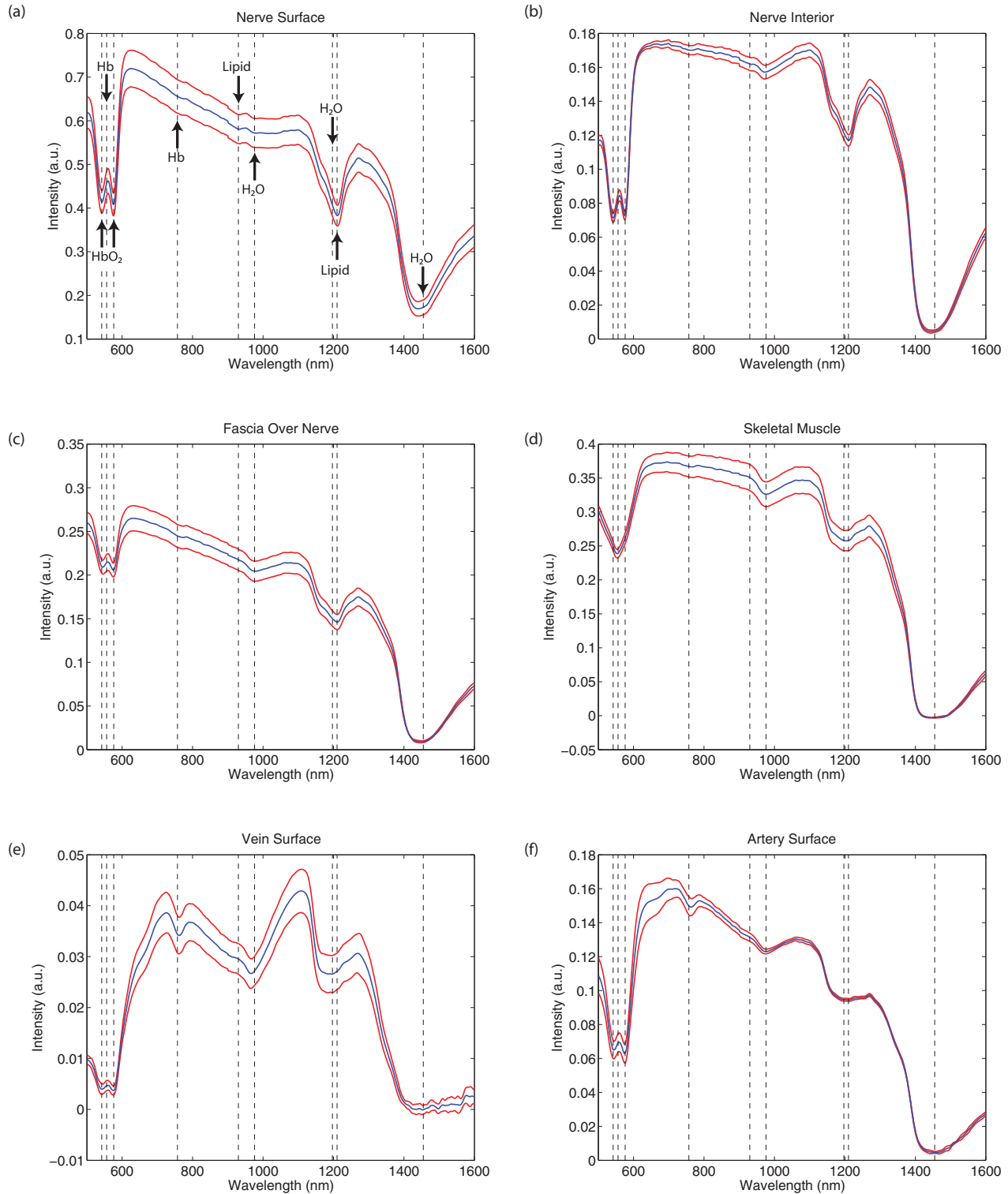


Fig. 2 Optical spectra acquired from tissues in the brachial plexus dissection, with the needle stylet positioned inside the needle cannula. One representative set of spectra that was acquired from a particular location in the dissection field is shown for each tissue structure. Spectra are presented as mean (blue; center) \pm SD (red; top/bottom). The standard deviations in the spectra provide an indication of the variability encountered with the stylet held in place by the practitioner. Spectra were acquired with the needle tip positioned (a) on the surface an exposed nerve, (b) inside a nerve, (c) on the fascia layer in contact with nerve, (d) on the cut surface of skeletal muscle, (e) on the surface of vein, and (f) on the surface of an artery. Specific wavelengths corresponding to selected absorption peaks are indicated with dashed lines. Oxy-hemoglobin: 542 and 576 nm; deoxy-hemoglobin: 557 and 757 nm; lipids: 930 and 1210 nm; water: 976, 1197, and 1455 nm.

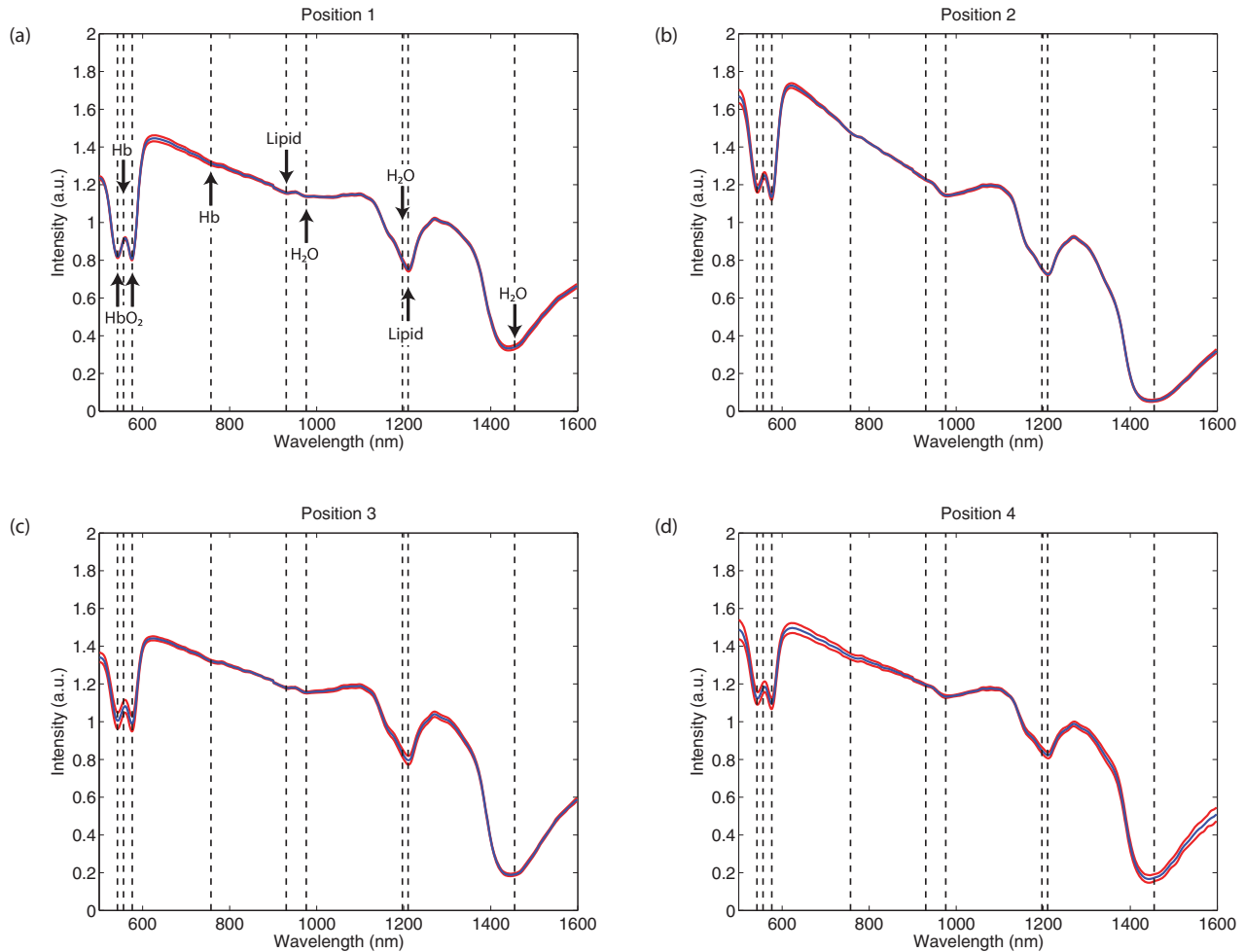


Fig. 3 Spectra from all positions on the surfaces of exposed nerves from which optical spectra were acquired. Spectra are presented as mean (blue) \pm SD (red). These plots provide qualitative indications of the variability in spectral shape encountered with the stylet tip at (a–d) four different positions. Specific wavelengths corresponding to selected absorption peaks are indicated with dashed lines. Oxy-hemoglobin: 542 and 576 nm; deoxy-hemoglobin: 557 and 757 nm; lipids: 930 and 1210 nm; water: 976, 1197, and 1455 nm.

when the stylet tip was positioned differently. For all four mean spectra acquired from the surfaces of nerves, prominent lipid absorption peaks at 1210 nm and very subtle ones at 930 nm were apparent. Prominent water absorption peaks at 1455 nm and more subtle ones at 976 nm were also apparent in all spectra. Absorption peaks consistent with oxy-hemoglobin were apparent in all four mean spectra acquired from the surfaces of nerves. However, with other spectra, such as those derived from muscle, hemoglobin absorption peaks differed with the location of the needle tip; oxy-hemoglobin absorption peaks were apparent in some while deoxy-hemoglobin absorption peaks were apparent in others (data not shown).

Absorption peaks corresponding to hemoglobin, water, and lipid were apparent in each of the first four components obtained with PCA [Fig. 4(a)]. By applying LDA to the principal component scores, two sets of spectrum classifiers (SC1 and SC2) were obtained. In a scatter plot of the spectrum classifiers, clusters corresponding to spectra acquired from different tissue structures were apparent [Fig. 4(b)]. In particular, spectrum classifiers corresponding to spectra acquired from nerve target regions and from inside nerves occupied a region largely distinct from those corresponding to spectra from adjacent tissues.

Spectrum classifiers corresponding to spectra acquired from the surfaces of veins and arteries and from inside skeletal muscle also derived from distinct regions.

4 Discussion

This pilot study demonstrated the feasibility of constructing a needle stylet with integrated optical fibers for acquiring spectra that span the visible and NIR wavelength ranges. The stylet diameter was sufficiently small to be compatible with a 20-gauge needle cannula. As such, only minor modifications would be required to make the stylet compatible with a wide range of needle cannulae used in peripheral nerve blocks, including ones that allow for electrical stimulation and ablation. The preliminary experiences of the practitioners during this study suggested that the presence of optical fibers and the resulting nonuniformity of the bevel surface of the stylet did not significantly change the resistance from tissues encountered during insertions or the mechanical properties of the stylet/needle combination.

It is known from spectroscopic studies with optical probes that the distance between the optical fibers that receive and collect light strongly affects the average distance traveled in

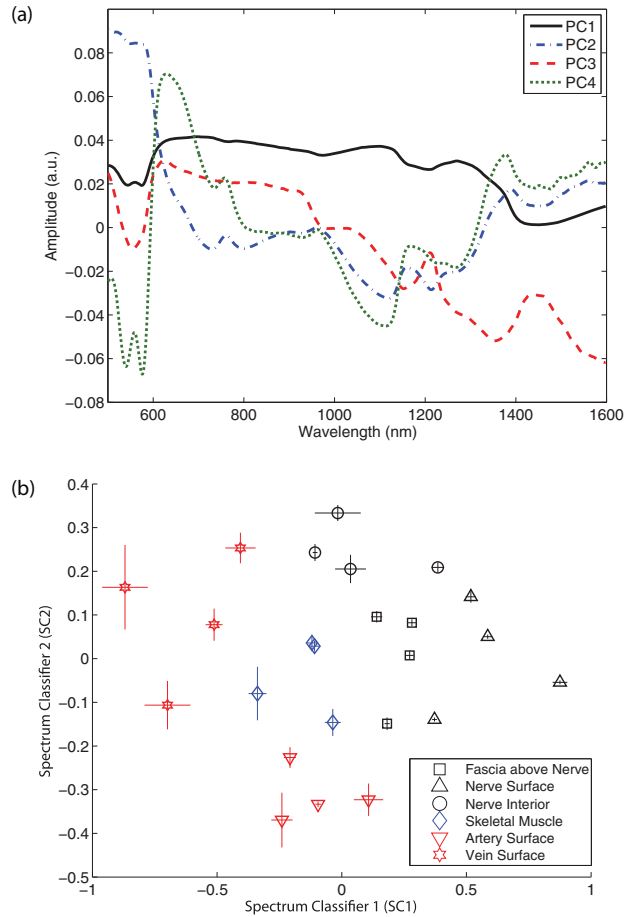


Fig. 4 (a) The first four principal components obtained by applying PCA to all spectra acquired in the study. (b) Representation of spectra with spectrum classifiers obtained with the PCA-LDA algorithm. Each point on the plot corresponds to an anatomical location from which spectra were acquired, displayed as a mean value (center) \pm SD (horizontal and vertical bars). Clusters of points that correspond to spectra acquired from different tissue structures are apparent.

tissue by the received light.⁴⁰ For smaller interfiber distances, received light travels less far in tissue and therefore experiences fewer absorption effects. In general, therefore, more prominent absorption peaks could be achieved with larger diameter (lower-gauge) stylets than for smaller diameter (higher-gauge) ones.

In the spectra acquired from the stylet demonstrated in this study, absorption peaks that were consistent with the presence of lipids, water, and hemoglobins could clearly be identified. The prominent lipid absorption peaks in spectra acquired from nerves likely had multiple morphological correlates. Intrafascicular structures, such as myelin sheaths, are known to be lipid rich.⁴⁹ Lipids can also be found in extrafascicular adipose cells contained within the epineurium, as well as extraneurally in the regions targeted during peripheral nerve blocks. In particular, >50% of the brachial plexus in the supraclavicular region is composed of fibrofatty connective tissue.⁵⁰ The prominence of the lipid absorption peaks can be expected to depend on the concentrations of water, collagen, and elastin, given that these chromophores have optical absorption peaks that partially overlap.⁵¹

The absorption peaks in the visible wavelength range were indicative of the presence of hemoglobins. In the case of spectra

acquired from skeletal muscle, there may have been additional contributions from myoglobins, which have very similar absorption spectra. During the course of the dissection, blood released from tissues migrated to some extent from one location to another. Caution must therefore be exercised when interpreting the prominence of hemoglobin absorption peaks. That said, the prominent hemoglobin absorption peaks observed in all spectra acquired from the surfaces of veins strongly suggests that the look-ahead distance of the stylet was sufficiently large to encompass part of the axillary vein lumen. In the case of spectra acquired from the surface of the axillary artery, most light may have scattered in the wall without entering the lumen.

The PCA-LDA algorithm allowed for an efficient representation of spectra acquired from different tissue structures. Because spectra were acquired from a small number of positions in a single cadaveric specimen, the scatter plot of the two spectrum classifiers provided only a preliminary indication of the extent to which tissue structures could be differentiated. A disadvantage of the PCA-LDA algorithm in this context is that the spectrum classifiers can be difficult to interpret in terms of physiological parameters. Several solutions to this inverse problem have been proposed. For instance, in the study of Nachabé et al., physiological and optical parameters were measured by fitting reflectance spectra to a model of light propagation based on diffusion theory.³⁹ In the context of PCA, each component score parameter is related to the concentrations of multiple chromophores and scattering coefficients in a nonlinear fashion.⁵²

The position of the needle tip relative to neural structures is critical to maximize the probability of successful outcomes and to minimize the probability of complications. Although proximity to the target nerve is important, intraneural injections can result in neurologic injury, particularly if injections are intrafascicular.⁵³ Optical reflectance spectroscopy provides information complementary to electrical stimulation and ultrasound; if it were found to provide robust contrast for contact between the needle tip and the nerve surface in humans, then it could increase procedural safety. Spectra acquired with the needle tip positioned intraneurally likely depend on the exact position of the needle tip relative to nerve fascicles and fibrofatty connective tissues. These differences will be explored in future studies.

Optical spectra acquired with a percutaneous needle insertion *in vivo* may differ from those acquired in this study with a dissection *ex vivo*. As a needle is inserted, it can compress tissue; as such, it can alter the optical properties.⁵⁴ Likewise, a needle can rupture small blood vessels that could lead to small accumulations of blood at the tip. In the context of a postmortem dissection, the alterations in tissue morphology that are induced by cell death or by the trauma associated with cutting operations could manifest spectroscopically.

Recent advances in fiber-optic and light-sensing technologies have enabled several different methods for optically interrogating tissues at the distal ends of needle cannulae. The results of this study indicate that optical reflectance spectroscopy, performed with optical fibers integrated into a needle stylet, could provide information relevant to nerve identification. As such, they motivate follow-up studies with percutaneous needle insertions *in vivo* to develop diagnostic algorithms based on optical spectra. In the context of peripheral nerve blocks, spectroscopic information could be complementary to ultrasound

images, providing molecular contrast that has been hitherto unavailable.

Acknowledgments

The authors gratefully acknowledge assistance with the swine dissection by Pellina Janson and Dr. Anton Razuvaev (Karolinska Hospital), and assistance with needle stylet design and development by Cor van der Vleuten (Philips Research), Frans van Gaal (VDL), and Ben Wassink (VDL). This paper benefited significantly from critical reviews by Dr. Micha Sommer (University Hospital Maastricht), Dr. Ke Wang (Philips Research), and Jasper Klewer (Philips Research).

References

- P. Raj, "Ancillary measures to assure success," *Reg. Anesth. Pain. Med.* **5**, 9–12 (1980).
- A. Perlas, A. Niazi, C. McCartney, V. Chan, D. Q. Xu, and S. Abbas, "The sensitivity of motor response to nerve stimulation and paresthesia for nerve localization as evaluated by ultrasound," *Reg. Anesth. Pain. Med.* **31**, 445–450 (2006).
- J. De Andrés, J. M. Alonso-Iñigo, X. Sala-Blanch, and M. A. Reina, "Nerve stimulation in regional anesthesia: theory and practice," *Best Pract. Res. Clin. Anaesthesiol.* **19**, 153–174 (2005).
- W. F. Urmev and J. Stanton, "Inability to consistently elicit a motor response following sensory paresthesia during interscalene block administration," *Anesthesiology* **96**, 552–554 (2002).
- A. Choyce, V. W. S. Chan, W. J. Middleton, P. R. Knight, P. Peng, and C. J. L. McCartney, "What is the relationship between paresthesia and nerve stimulation for axillary brachial plexus block?," *Reg. Anesth. Pain. Med.* **26**, 100–104 (2001).
- T. Grau, S. Fatehi, J. Motsch, and E. Bartussek, "Survey on current practice of regional anaesthesia in Germany, Austria, and Switzerland. Part 2: use, success rates and techniques," *Anaesthetist* **53**, 847–855 (2004).
- A. P. Baranowski and C. E. Pither, "A comparison of 3 methods of axillary brachial-plexus anesthesia," *Anaesthesia* **45**, 362–365 (1990).
- P. Marhofer and V. W. S. Chan, "Ultrasound-guided regional anesthesia: current concepts and future trends," *Anesth. Analg.* **104**, 1265–1269 (2007).
- P. E. Bigeleisen, N. Moayeri, and G. J. Groen, "Extraneural versus intraneural stimulation thresholds during ultrasound-guided supraclavicular block," *Anesthesiology* **110**, 1235–1243 (2009).
- G. Y. Wong, D. L. Brown, G. M. Miller, and D. R. Cahill, "Defining the cross-sectional anatomy important to interscalene brachial plexus block with magnetic resonance imaging," *Reg. Anesth. Pain. Med.* **23**, 77–80 (1998).
- S. K. Mukherji, A. Wagle, D. M. Armao, and S. Dogra, "Brachial plexus nerve block with CT guidance for regional pain management: initial results," *Radiology* **216**, 886–890 (2000).
- M. Nishiyama, K. Naganuma, and Y. Amaki, "A new approach for brachial plexus block under fluoroscopic guidance," *Anesth. Analg.* **88**, 91–97 (1999).
- W. A. Reed, M. F. Yan, and M. J. Schnitzer, "Gradient-index fiber-optic microprobes for minimally invasive *in vivo* low-coherence interferometry," *Opt. Lett.* **27**, 1794–1796 (2002).
- D. T. Raphael, J. Zhang, Y. P. Zhang, Z. P. Chen, C. Miller, and L. Zhou, "OCT/PS-OCT imaging of brachial plexus neurovascular structures," *Proc. SPIE* **5312**, 388–395 (2004).
- D. T. Raphael, C. H. Yang, N. Tresser, J. G. Wu, Y. P. Zhang, and L. Rever, "Images of spinal nerves and adjacent structures with optical coherence tomography: preliminary animal studies," *J. Pain* **8**, 767–773 (2007).
- S. A. Boppart, B. E. Bouma, C. Pitris, J. F. Southern, M. E. Brezinski, and J. G. Fujimoto, "Intraoperative assessment of microsurgery with three-dimensional optical coherence tomography," *Radiology* **208**, 81–86 (1998).
- N. M. Fried, S. Rais-Bahrami, G. A. Lagoda, Y. Chuang, A. L. Burnett, and L. M. Su, "Imaging the cavernous nerves in the rat prostate using optical coherence tomography," *Lasers Surg. Med.* **39**, 36–41 (2007).
- S. Rais-Bahrami, A. W. Levinson, N. M. Fried, G. A. Lagoda, A. Hristov, Y. Chuang, A. L. Burnett, and L. M. Su, "Optical coherence tomography of cavernous nerves: a step toward real-time intraoperative imaging during nerve-sparing radical prostatectomy," *Urology* **72**, 198–204 (2008).
- L. B. Boyette, M. A. Reardon, A. J. Mirelman, T. D. Kirkley, J. J. Lysiak, J. B. Tuttle, and W. D. Steers, "Fiberoptic imaging of cavernous nerves *in vivo*," *J. Urology* **178**, 2694–2700 (2007).
- J. Sun, C. Shu, B. Appiah, and R. Drezek, "Needle-compatible single fiber bundle image guide reflectance endoscope," *J. Biomed. Opt.* **15**, 040502 (2010).
- A. N. Bashkatov, E. A. Genina, V. I. Kochubey, and V. V. Tuchin, "Optical properties of human skin, subcutaneous and mucous tissues in the wavelength range from 400 to 2000 nm," *J. Phys. D Appl. Phys.* **38**, 2543–2555 (2005).
- G. J. Liese, W. Pong, and D. E. Brandt, "Fiber-optic stylet for needle tip localization," *Appl. Opt.* **24**, 3125–3126 (1985).
- I. J. Bigio, S. G. Bown, G. Briggs, C. Kelley, S. Lakhani, D. Pickard, P. M. Ripley, I. G. Rose, and C. Saunders, "Diagnosis of breast cancer using elastic-scattering spectroscopy: preliminary clinical results," *J. Biomed. Opt.* **5**, 221–228 (2000).
- D. A. Benaron, I. H. Parachikov, S. Friedland, R. Soetikno, J. Brock-Utne, P. J. A. van der Starre, C. Nezhat, M. K. Terris, P. G. Maxim, J. J. L. Carson, M. K. Razavi, H. B. Gladstone, E. F. Fincher, C. P. Hsu, F. L. Clark, W. F. Cheong, J. L. Duckworth, and D. K. Stevenson, "Continuous, noninvasive, and localized microvascular tissue oximetry using visible light spectroscopy," *Anesthesiology* **100**, 1469–1475 (2004).
- D. A. Benaron, I. H. Parachikov, W. F. Cheong, S. Friedland, B. E. Rubinsky, D. M. Otten, F. W. H. Liu, C. J. Levinson, A. L. Murphy, J. W. Price, Y. Talmi, J. P. Weersing, J. L. Duckworth, U. B. Horchner, and E. L. Kermit, "Design of a visible-light spectroscopy clinical tissue oximeter," *J. Biomed. Opt.* **10**, 044005 (2005).
- R. L. P. van Veen, A. Amelink, M. Menke-Pluyers, C. van der Pol, and H. Sterenberg, "Optical biopsy of breast tissue using differential path-length spectroscopy," *Phys. Med. Biol.* **50**, 2573–2581 (2005).
- S. C. Kanick, C. van der Leest, J. Aerts, H. C. Hoogsteden, S. Kascakova, H. Sterenberg, and A. Amelink, "Integration of single-fiber reflectance spectroscopy into ultrasound-guided endoscopic lung cancer staging of mediastinal lymph nodes," *J. Biomed. Opt.* **15**, 017004 (2010).
- C. Lubawy and N. Ramanujam, "Endoscopically compatible near-infrared photon migration probe," *Opt. Lett.* **29**, 2022–2024 (2004).
- B. Yu, E. S. Burnside, G. A. Sisney, J. M. Harter, C. Zhu, A. H. Dhalla, and N. Ramanujam, "Feasibility of near-infrared diffuse optical spectroscopy on patients undergoing image-guided core-needle biopsy," *Opt. Express* **15**, 7335–7350 (2007).
- S. M. Latyev, D. V. Shpakov, V. A. Volchkov, E. A. Puisha, and O. Mollenkauer, "The possibility of identifying the epidural space in anesthesiological practice by optical methods," *J. Opt. Technol.* **69**, 292–294 (2002).
- C.-K. Ting, M.-Y. Tsou, P.-T. Chen, K.-Y. Chang, S. Mandell, K.-H. Chan, and Y. Chang, "A new technique to assist epidural needle placement," *Anesthesiology* **112**, 1128–1135 (2010).
- C. F. Zhu, E. S. Burnside, G. A. Sisney, L. R. Salkowski, J. M. Harter, B. Yu, and N. Ramanujam, "Fluorescence spectroscopy: an adjunct diagnostic tool to image-guided core needle biopsy of the breast," *IEEE Trans. Biomed. Eng.* **56**, 2518–2528 (2009).
- D. Capellaro and N. S. Kapany, "A hypodermic probe using fibre optics," *Nature* **191**, 927–928 (1961).
- S. S. Bu, S. F. Xie, J. Lu, X. J. Cao, B. R. Xiang, and Y. Ye, "Short communication: the preliminary research of identifying motor and sensory fascicles using near infrared diffuse reflectance spectroscopy in combination with soft independent modelling of class analogy," *J. Near Infrared Spec.* **16**, 431–436 (2008).
- S. F. Xie, B. R. Xiang, S. S. Bu, X. J. Cao, Y. Ye, J. Lu, and H. S. Deng, "Rapid identification of anterior and posterior root of cauda equina nerves by near-infrared diffuse reflectance spectroscopy," *J. Biomed. Opt.* **14**, 024005 (2009).
- A. Abdo and M. Sahin, "NIR light penetration depth in the rat peripheral nerve and brain cortex," in *Proc. of 2007 Annual Int. Conf. of IEEE Eng. in Med. and Biol. Soc.*, Vols. 1–16, 1723–1725 (2007).

37. H. Radhakrishnan, A. Senapati, D. Kashyap, Y. B. Peng, and H. Liu, "Light scattering from rat nervous system measured intraoperatively by near-infrared reflectance spectroscopy," *J. Biomed. Opt.* **10**, 051405 (2005).
38. H. Radhakrishnan, A. Senapati, Y. B. Peng, D. Kashyap, and H. L. Liu, "Near infrared reflectance spectroscopy as a novel method to detect demyelination in rat sciatic nerve *in vivo*," *Proc. SPIE* **5686**, 477–486 (2005).
39. R. Nachabé, B. H. W. Hendriks, A. E. Desjardins, M. van der Voort, M. B. van der Mark, and H. J. C. M. Sterenborg, "Estimation of lipid and water concentrations in scattering media with diffuse optical spectroscopy from 900 to 1600 nm," *J. Biomed. Opt.* **15**, 037015 (2010).
40. D. Arifler, C. MacAulay, M. Follen, and R. Richards-Kortum, "Spatially resolved reflectance spectroscopy for diagnosis of cervical precancer: Monte Carlo modeling and comparison to clinical measurements," *J. Biomed. Opt.* **11**, 064027 (2006).
41. P. Crow, B. Barrass, C. Kendall, M. Hart-Prieto, M. Wright, R. Persad, and N. Stone, "The use of Raman spectroscopy to differentiate between different prostatic adenocarcinoma cell lines," *Br. J. Cancer* **92**, 2166–2170 (2005).
42. L. Notingher, G. Jell, P. L. Notingher, I. Bisson, O. Tsigkou, J. M. Polak, M. M. Stevens, and L. L. Hench, "Multivariate analysis of Raman spectra for *in vitro* non-invasive studies of living cells," *J. Mol. Struct.* **744**, 179–185 (2005).
43. F. L. Martin, M. J. German, E. Wit, T. Fearn, N. Ragavan, and H. M. Pollock, "Identifying variables responsible for clustering in discriminant analysis of data from infrared microspectroscopy of a biological sample," *J. Comput. Biol.* **14**, 1176–1184 (2007).
44. R. O. Duda, P. E. Hart, and D. G. Stork, *Pattern Classification*, Wiley, Hoboken, NJ (2001).
45. K. A. Schenkman, D. R. Marble, E. O. Feigl, and D. H. Burns, "Near-infrared spectroscopic measurement of myoglobin oxygen saturation in the presence of hemoglobin using partial least-squares analysis," *Appl. Spectrosc.* **53**, 325–331 (1999).
46. R. R. Anderson, W. Farinelli, H. Laubach, D. Manstein, A. N. Yaroslavsky, J. Gubeli, K. Jordan, G. R. Neil, M. Shinn, W. Chandler, G. P. Williams, S. V. Benson, D. R. Douglas, and H. F. Dylla, "Selective photothermolysis of lipid-rich tissues: A free electron laser study," *Lasers Surg. Med.* **38**, 913–919 (2006).
47. V. R. Kondepati, H. M. Heise, and J. Backhaus, "Recent applications of near-infrared spectroscopy in cancer diagnosis and therapy," *Anal. Bioanal. Chem.* **390**, 125–139 (2008).
48. L. H. Kou, D. Labrie, and P. Chylek, "Refractive-indexes of water and ice in the 0.65-Mu-M to 2.5-Mu-M spectral range," *Appl. Opt.* **32**, 3531–3540 (1993).
49. M. J. Brown, D. E. Pleasure, and A. K. Asbury, "Microdissection of peripheral-nerve—collagen and lipid distribution with morphological correlation," *J. Neurol. Sci.* **29**, 361–369 (1976).
50. N. Moayeri, P. E. Bigeleisen, and G. J. Groen, "Quantitative architecture of the brachial plexus and surrounding compartments, and their possible significance for plexus blocks," *Anesthesiology* **208**, 299–304 (2008).
51. C.-L. Tsai, J.-C. Chen, and W.-J. Wang, "Near-infrared absorption property of biological soft tissue constituents," *J. Med. Biol. Eng.* **21**, 7–14 (2001).
52. G. Zonios, L. T. Perelman, V. M. Backman, R. Manoharan, M. Fitzmaurice, J. Van Dam, and M. S. Feld, "Diffuse reflectance spectroscopy of human adenomatous colon polyps *in vivo*," *Appl. Opt.* **38**, 6628–6637 (1999).
53. A. Hadzic, F. Dilberovic, S. Shah, A. Kulenovic, E. Kapur, A. Zaciragic, E. Cosovic, E. Vuckovic, K. A. Divanovic, Z. Mornjakovic, D. M. Thys, and A. C. Santos, "Combination of intraneural injection and high injection pressure leads to fascicular injury and neurologic deficits in dogs," *Reg. Anesth. Pain. Med.* **29**, 417–423 (2004).
54. E. K. Chan, B. Sorg, D. Protsenko, M. O'Neil, M. Motamedi, and A. J. Welch, "Effects of compression on soft tissue optical properties," *IEEE J. Sel. Top. Quantum Electron.* **2**, 943–950 (1996).